Optical Society of America. Partha P. Banerjee, Dongquing Cao, and Ting-Chung Poon, "Notch Spatial Filtering with an Acousto-Optic Modulator," Appl. Opt. 37, 7532-7537 (1998). doi: 10.1364/ao.37.007532

Notch spatial filtering with an acousto-optic modulator

Partha P. Banerjee, Dongquing Cao, and Ting-Chung Poon

The role of acousto-optic (AO) modulators in programmable real-time image processing has recently been demonstrated. For fully investigating the image-processing capabilities of the AO modulator, general techniques to derive spatial transfer functions are needed for a variety of physical situations. We develop a technique to determine the spatial transfer functions numerically for various cases of beam incidence on an AO modulator. Normal incidence and incidence at twice the Bragg angle are investigated as examples for which double-sided and single-sided notch spatial filtering, respectively, are achieved. The observed spatial-filtering characteristics are reconciled with simple intuitive physical arguments. © 1998 Optical Society of America

OCIS codes: 070.1060, 100.1160.

1. Introduction

Most of the methods for real-time programmable image processing and optical correlation employ two-dimensional (2-D) spatial light modulators (SLM's). Popular SLM's include liquid-crystal televisions (LCTV's), liquid-crystal light valves (LCLV's), and magneto-optic devices (MOD's).[1–3] Because the resolution required for accurate representation of the image or image transforms is extremely high, the cost of SLM's that meet the specifications is also prohibitively high. Even though the use of SLM's enables the image-processing system to be real time and programmable, phase uniformity and contrast ratio are critical considerations in the design of the SLM to make them practical and useful. Conversely, acousto-optic modulators (AOM's) are well-developed mature one-dimensional (1-D) devices and have been used mainly for 1-D optical signal processing.[4–6] The use of AOM's for image processing has recently been explored.[7–9] The novel feature of the technique is that lensless 2-D optical image processing can be achieved. In fact, the 2-D optical image interacts with the sound fields in the AOM's. The scattering or the diffraction of the 2-D optical image actually carries the processed versions of the original 2-D input image. Processing is thus performed in real time, as the AOM is a real-time device. In addition, the processing operation is programmable, as the sound amplitude or the sound frequency within the AOM can be varied electronically; hence the input image can be modified accordingly.

Insights into acousto-optic (AO) image spatial filtering have been obtained through the use of spatial transfer functions. Indeed, the spatial transfer function for an AO modulator working in the Bragg regime that shows the spatial-frequency selectivity of both the diffracted and the undiffracted orders has recently been derived and studied.[7–11] In short, under certain conditions, the undiffracted order has the characteristics of spatial high-pass filtering, while the transfer function for the diffracted order shows low-pass characteristics. To develop more and diversified spatial-filtering operations, techniques to compute spatial transfer functions under a variety of physical situations—such as different nominal angles of optical incidence, the utilization of different diffracted orders at the output, etc.—are needed. Whereas analytical solutions are usually not available for many physical situations mentioned, recourse to numerical solutions is often sought. Pieper and Poon[12] proposed a general methodology for calculating the AO spatial transfer functions by using a multiple plane-wave scattering technique. However, in their formalism, the effect of diffraction that is due to propagation through the AOM has been neglected. In Section 2 of this paper we propose another technique to compute spatial transfer functions wherein spatial propagation has been taken into account. In Section 3 we then employ the proposed formalism to investigate two situations as ex-

P. P. Banerjee (banerjee@ece.uah.edu) and D. Cao are with the Department of Electrical and Computer Engineering, University of Alabama in Huntsville, Huntsville, Alabama 35899; T.-C. Poon (tcpoon@vt.edu) is with the Department of Electrical Engineering, Virginia Polytechnic Institute, Blacksburg, Virginia 24061.

Received 12 February 1998.
0003-6935/98/327532-06$15.00/0

amples: normal incidence and incidence at twice the Bragg angle.

2. Basic Formulation and Derivation of the Acousto-Optic Interaction Equations

We start with the wave equation for a 2-D optical field $\mathbf{E}(x, z, t)$, polarized in the y direction, in the AO medium:

$$\frac{\partial^2 \mathbf{E}}{\partial t^2} - v^2 \nabla^2 \mathbf{E} = -\left(\frac{\epsilon'}{\epsilon_0}\right) \frac{\partial^2 \mathbf{E}}{\partial t^2}, \tag{1}$$

where v is the light velocity in the AO medium, ϵ_0 is the intrinsic permittivity in the AO medium, and ϵ' represents the acoustically driven perturbation in the permittivity. The optical field in the AO cell can be expressed as

$$\mathbf{E}(x, z; t) = \sum_m \mathrm{Re}\{\psi_m(x, z) \times \exp[j(\omega_m t - k_{mx} x - k_{mz} z)]\}\hat{a}_y. \tag{2}$$

In Eq. (2), ψ_m represents the complex amplitude of the mth diffracted order, ω_m is the temporal frequency of the mth-order light, and k_{mx}, k_{mz} represent the x and z components, respectively, of the propagation constants of the mth scattered order. Also, $\hat{a}_y$ is the unit vector along the y direction. From a simple heuristic treatment of acousto-optics, it is readily seen that

$$\omega_m = \omega + m\Omega, \tag{3}$$

where ω is the original angular frequency of the incident light, ω_m is the optical frequency of the mth-order diffracted light beam, and the Bragg angle is

$$\phi_B \cong \frac{K}{2k} = \frac{\lambda_0}{2\Lambda n_0}, \qquad \phi_m \cong \phi_{\mathrm{inc}} + mK/k, \tag{4}$$

where λ_0 is the light wavelength in free space, n_0 is the intrinsic refractive index of the AO medium, Λ is the sound wavelength in the AO medium, k represents the propagation constant of light in the AO medium, and K is the propagation constant of the sound. Hence $k_{mx} = k \sin \phi_m$ and $k_{mz} = k \cos \phi_m$.

Let us assume a sound field propagating along the positive x direction with an amplitude $S_e(x, z)$ in the AO medium:

$$\epsilon' = \epsilon_0 C \,\mathrm{Re}[S_e(x, z) \exp j(\Omega t - Kx)], \tag{5}$$

where C is the AO interaction constant and Ω is the sound angular frequency. We now assume that $S_e(x, z) = A$, a constant for simplicity. On substituting Eqs. (2) and (5) into Eq. (1) and gathering the coefficients of $\exp[j(\omega + m\Omega)t]$, we obtain

$$\frac{\partial^2 \psi_m}{\partial x^2} - 2j\left(k_{mx} \frac{\partial \psi_m}{\partial x} + k_{mz} \frac{\partial \psi_m}{\partial z}\right) + \left(\frac{k^2 C}{2}\right) \times (A\psi_{(m-1)} \exp\{-j[k_{(m-1)z} - k_{mz}]z\} + A^* \psi_{(m+1)} \exp\{-j[k_{(m+1)z} - k_{mz}]z\}) + \frac{\partial^2 \psi_m}{\partial z^2} = 0. \tag{6}$$

If we assume a slow variation of ψ_m with respect to z, i.e.,

$$\left|\frac{\partial^2 \psi_m}{\partial z^2}\right| \ll \left|k_{mz} \frac{\partial \psi_m}{\partial z}\right|, \tag{7}$$

Eq. (6) becomes

$$\frac{\partial^2 \psi_m}{\partial x^2} - 2j\left(k_{mx} \frac{\partial \psi_m}{\partial x} + k_{mz} \frac{\partial \psi_m}{\partial z}\right) + \left(\frac{k^2 C}{2}\right) \times (A\psi_{(m-1)} \exp\{-j[k_{(m-1)z} - k_{mz}]z\} + A^* \psi_{(m+1)} \exp\{-j[k_{(m+1)z} - k_{mz}]z\}) = 0. \tag{8}$$

Finally, on Fourier-transforming Eq. (9), we find that the angular plane-wave spectra of the various diffracted orders evolve according to

$$\frac{\partial \hat{\psi}_m}{\partial z} = j \frac{(k_x^2 + 2k_x k_{mx})}{2k_{mz}} \hat{\psi}_m - jD\hat{\psi}_{m+1} - jE\hat{\psi}_{m-1}, \tag{9}$$

where

$$D = (kCA^*/4)\exp\{-jk[\cos(\phi_{m+1}) - \cos(\phi_m)]z\}, \tag{10a}$$

$$E = (kCA/4)\exp\{-jk[\cos(\phi_{m-1}) - \cos(\phi_m)]z\}. \tag{10b}$$

The angular spectra of the various scattered orders $\hat{\psi}_m$ are defined according to the Fourier transform relation, which is given as

$$\hat{\psi}_m(k_x, z) = F_x[\psi_m(x, z)] = \int_{-\infty}^{\infty} \psi_m(x, z) \exp(jk_x x)\mathrm{d}x. \tag{11}$$

In Eq. (9), the first term in parentheses on the right-hand side represents the propagational diffraction effect. The second and third terms on the right-hand side model the AO interaction.

For nominal Bragg incidence ($\phi_{\mathrm{inc}} = \phi_B$), only the zeroth and negative-first diffracted orders exist, and exact analytical expressions for the interaction transfer functions can be determined. For instance, from Eq. (9) we obtain

$$\frac{\partial \hat{\psi}_0}{\partial z} = \frac{j(k_x^2 + 2k_x k_{0x})}{2k_{0z}} \hat{\psi}_0 - jE\hat{\psi}_{-1}, \tag{12}$$

$$\frac{\partial \hat{\psi}_{-1}}{\partial z} = \frac{j(k_x^2 + 2k_x k_{-1x})}{2k_{-1z}} \hat{\psi}_{-1} - jD\hat{\psi}_0, \tag{13}$$

where $k_{0x} = k \sin \phi_B$, $k_{0z} = k \cos \phi_B$, $k_{-1x} = -k \sin \phi_B$, and $k_{-1z} = k \cos \phi_B$. Here D and E are simplified to $D = kCA^*/4$ and $E = kCA/4$, respectively, because $\phi_{\text{inc}} = \phi_B$ and $\phi_{-1} = \phi_0 - 2\phi_B = -\phi_B$. From Eqs. (12) and (13) we can obtain the spatial transfer functions analytically for undiffracted and first diffracted orders as

$$H_0(k_x, z = L) = \exp\left[j\left(\frac{k_x^2 L}{2k}\right)\right]\left\{\cos\left[\left(\frac{k_x k_{0x} L}{k}\right)^2 + \left(\frac{\alpha}{2}\right)^2\right]^{1/2} + \left(\frac{jk_x k_{0x} L}{k}\right)\frac{\sin\left[\left(\frac{k_x k_{0x} L}{k}\right)^2 + \left(\frac{\alpha}{2}\right)^2\right]^{1/2}}{\left[\left(\frac{k_x k_{0x} L}{k}\right)^2 + \left(\frac{\alpha}{2}\right)^2\right]^{1/2}}\right\}, \tag{14}$$

$$H_1(k_x, z = L) = \exp\left[j\left(\frac{k_x^2 L}{2k}\right)\right]\left(-j\,\frac{\alpha}{2}\right)\frac{\sin\left[\left(\frac{k_x k_{0x} L}{k}\right)^2 + \left(\frac{\alpha}{2}\right)^2\right]^{1/2}}{\left[\left(\frac{k_x k_{0x} L}{k}\right)^2 + \left(\frac{\alpha}{2}\right)^2\right]^{1/2}}, \tag{15}$$

where $\alpha = kC|A|L/2$ represents the peak phase delay that is due to the AO interaction, which is proportional to the sound pressure. Here L is the AO interaction length. Also note that $k_{0x}L/k = Q\Lambda/4\pi$, where $Q = 2\pi\lambda_0 L/\Lambda^2 n_0$ is the Klein–Cook parameter. The propagational diffraction effect through the length of the AO cell is represented by the phase term $\exp[j(k_x^2 L/2k)]$. The remaining terms in Eqs. (14) and (15) characterize the AO interaction process. Equations (14) and (15) show that, in essence, the propagational diffraction effects are decoupled from the AO interaction process. Note that in Pieper and Poon's formalism[12] the term corresponding to propagational diffraction effects was absent. The term is important when the AO interaction length is large.[13] Plots of the transfer functions appear in Refs. 8 and 9, and the physical explanation for the nature of the variation as a function of spatial frequency is given in Ref. 9. The undiffracted order shows a high-pass spatial frequency response, whereas the diffracted order shows low-pass characteristics.

3. Determination of Spatial Transfer Functions

As we have pointed out, analytical solutions are often not available in acousto-optics; hence it is important to obtain numerical spatial transfer functions to gain insights into image-processing applicatons. In this section we discuss the procedure for determining the transfer functions. It involves (i) solving the set of coupled equations from Eq. (9) that are pertinent to a specific physical situation by use of a certain initial incident spectrum $\hat{\psi}_{\text{inc}}(k_x)$, (ii) evaluating the spectra of the scattered optical fields at the exit of the AO modulator, and finally (iii) calculating the spatial transfer functions for each diffracted order by determination of the ratio of the output spectrum of the specific order to the incident spectrum. We compute the transfer functions for two specific cases as examples: when the incident-light profile (or image) is nominally at normal incidence and when it is incident at twice the Bragg angle. We also indicate the spatial-filtering characteristics of each of the transfer functions and give a physical reason to justify our calculated results.

A. Acousto-Optic Interaction for Normal Incidence: Double-Sided Notch Filtering

In the first example we consider that the incident beam is at normal incidence. The schematic diagram for this case is shown in Fig. 1. Generally, most of the incident intensity is diffracted to the first and the negative-first diffracted orders; therefore we consider only the coupling effect between the two first-order diffracted beams and the undiffracted order.

From Eqs. (9) and (10) we can obtain the following coupled equations that describe the evolution of the zeroth, first, and negative-first orders:

$$\frac{\partial\hat{\psi}_0}{\partial z} = \frac{jk_x^2}{2k}\hat{\psi}_0 - \frac{j\alpha}{2L}\exp(jk\delta z)\hat{\psi}_1 - \frac{j\alpha}{2L} \times \exp(jk\delta z)\hat{\psi}_{-1}, \tag{16}$$

$$\frac{\partial\hat{\psi}_1}{\partial z} = \frac{j(k_x^2 + 4k\phi_B k_x)}{2k}\hat{\psi}_1 - \frac{j\alpha}{2L} \times \exp(-jk\delta z)\hat{\psi}_0, \tag{17}$$

$$\frac{\partial\hat{\psi}_{-1}}{\partial z} = \frac{j(k_x^2 - 4k\phi_B k_x)}{2k}\hat{\psi}_{-1} - \frac{j\alpha}{2L} \times \exp(-jk\delta z)\hat{\psi}_0, \tag{18}$$

where $\delta = 1 - \cos(2\phi_B)$ and $\hat{\psi}_0$, $\hat{\psi}_1$, and $\hat{\psi}_{-1}$ are the spatial spectra for the zeroth, first, and negative-first orders, respectively. The quantities α, L, k, k_x, and ϕ_B are the same as defined above. Since the analytical solutions of these Eqs. (16)–(18) are difficult to obtain directly, numerical calculations are performed instead. The numerical calculation results are shown in Fig. 2. The main parameters for the calculation are the sound frequency of $F = 55$ MHz, the

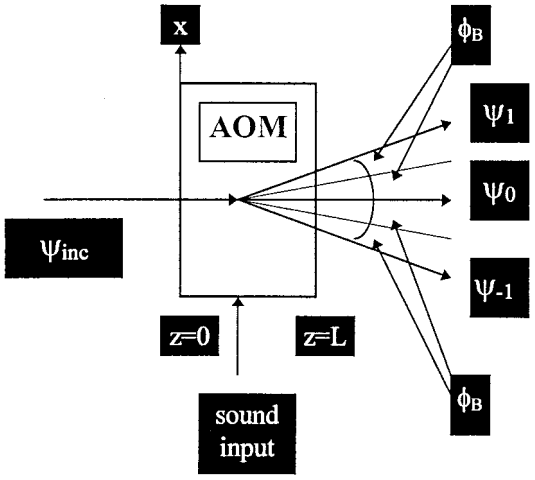

Fig. 1. Configuration showing light at normal incidence during AO interaction, along with the diffracted orders.

AO interaction length of $L = 62.5$ mm, the light wavelength of $\lambda_0 = 632.8$ nm, and the Klein–Cook parameter of $Q \approx 28$. These parameters are chosen to match our earlier experimental conditions with AO cells for image processing, as reported in Refs. 7–9. Since the AO system is linear,[12] the transfer function does not depend on the input condition. To evaluate the transfer function, we take a rectangular function $\mathrm{rect}(x/2a)$ and a Gaussian function $\exp\{-[x^2/(a/2)^2]\}$ as the incident images, where $a \approx 1$ mm. First, from Eqs. (16)–(18), the output spectrum profiles of the three orders are obtained by use of a simple space-matching algorithm. The initial conditions are $\hat{\psi}_0(k_x, z = 0) = F_x[\psi_{inc}(x)] = \hat{\psi}_{inc}(k_x)$, $\hat{\psi}_1(k_x, z = 0) = 0$, and $\hat{\psi}_{-1}(k_x, z = 0) = 0$. Then the ratios of the three output spectra at $z = L$ with the spectrum of the incident object are numerically calculated. We define the transfer functions for interaction as $H_i(k_x) = \hat{\psi}_i(k_x, z = L)/\hat{\psi}_{inc}(k_x)$, $i = 0, \pm 1$. The results show that the transfer functions indeed do not depend on the incident object, which is expected for a linear coupled system, and serve as a check of our numerical calculations. Care was taken to avoid computational difficulties around the zeros of the Fourier transform of the incident profile, e.g., the rect function. Figure 2(a) shows the magnitude curves of the undiffracted transfer-function profile at $\alpha = 0.6\pi$ and $\alpha = 0.8\pi$, respectively. The corresponding curves for the transfer functions of the positive–negative-first orders are shown in Figs. 2(b) and 2(c), respectively. Figure 2(a) shows that, for the undiffracted order, the transfer function of normal-incidence AO interaction has notch-filtering characteristics. We have found that the notch positions [$k_x \approx \pm 4.3 \times 10^4$ (1 m^{-1})] correspond to the angular plane-wave components traveling along $\pm\phi_B$. Hence the notch positions are programmable by electronic adjustment of the sound frequency. This can be explained physically as follows. Since the incident image has an angular spectrum, the plane-wave components traveling around $\pm\phi_B$ will be diffracted into positive–negative-first orders [see the corresponding high

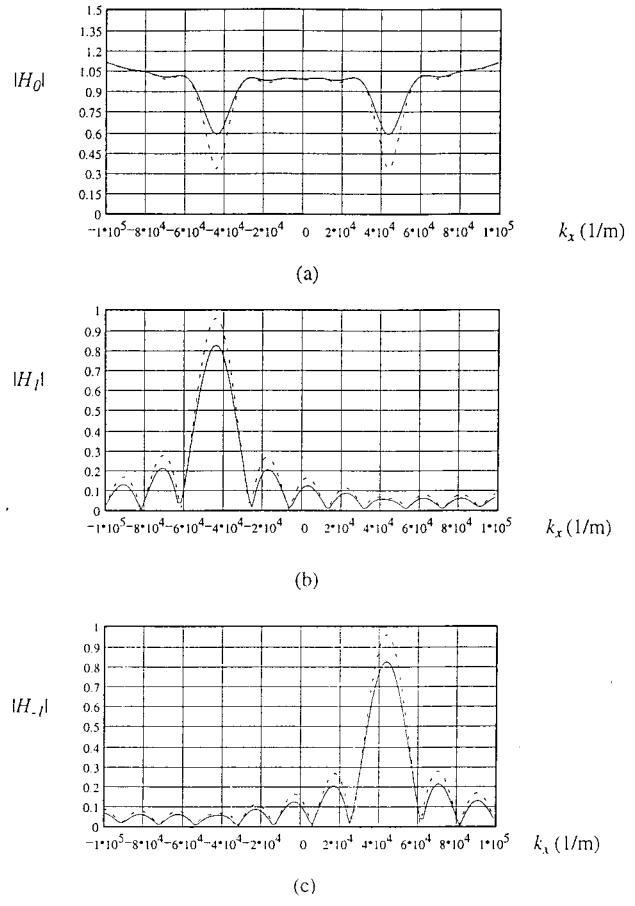

Fig. 2. Numerical calculation results for the transfer-function graphs for the case of normal incidence and for $Q = 28$, $\Lambda = 72$ μm, and $\lambda_0 = 632.8$ nm. Dashed curve, $\alpha = 0.8\pi$; solid curve, $\alpha = 0.6\pi$. (a) Zeroth order, (b) positive-first diffracted order, and (c) negative-first diffracted order.

peaks in the positive–negative-first-order transfer functions in Figs. 2(b) and 2(c)], leaving less light intensity in the undiffracted order [the notches in Fig. 2(a)]. Furthermore, the notch depth is programmable as well, since for higher α more light should be diffracted into positive–negative first orders. Figure 2 shows indeed that the notch at $\alpha = 0.8\pi$ is deeper than that at $\alpha = 0.6\pi$. The notch width can effectively be changed when one changes the Q value of the AO cell. These programmable characteristics suggest that the AO notch filtering has strong advantages in real-time image processing.

From Fig. 2(a) and from the physical explanation above, we speculate that the magnitude of the undiffracted-order transfer function of normal incidence can be approximated as

$$|H_0(k_x, z)| = [1 - |H_1(k_x - k\phi_B, z)|^2 - |H_{-1}(k_x + k\phi_B, z)|^2]^{1/2}, \quad (19)$$

where H_0 is the undiffracted-order transfer function of normal incidence and H_1 and H_{-1} are the transfer functions of the positive–negative first orders for Bragg incidence [see Eqs. (14) and (15)]. The argu-

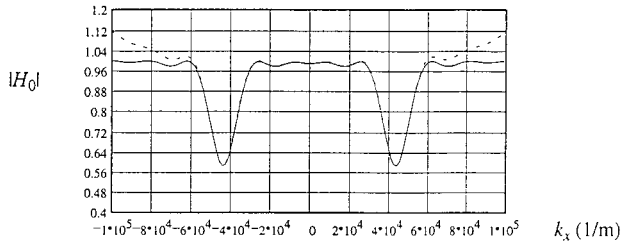

Fig. 3. Comparison between the computed zeroth-order transfer function (dashed curve) and the guessed analytical solution (solid curve) in the case of normal incidence. The parameters are $\alpha = 0.8\pi$, $Q = 28$, $\Lambda = 72$ μm, and $\lambda_0 = 632.8$ nm.

ments $\pm k\phi_B$ of H_1 and H_{-1} represent the shift of the transfer functions as the incident angle is now zero (corresponding to normal incidence) instead of being at the Bragg angle. The profile of $|H_0|$, according to Eq. (19), is obtained and is shown in Fig. 3, where α is equal to 0.6π. We can see that the profile matches well with the result obtained by use of the numerical iterative calculation method. We note that, however, at higher spatial frequencies the numerical solutions tend to deviate from the analytical solution. This is due to the number of steps taken along z during the numerical calculations. As the step size is increased, the numerical solution converges to 1 for large $|k_x|$. We point out that the prediction of the transfer function was made possible because it could be numerically evaluated easily with the procedure described above.

B. Acousto-Optic Interaction for Incidence at Twice the Bragg Angle: Single-Sided Notch Filtering

Appreciable power transfer between two orders is possible not only for Bragg incidence of the light on the AO cell but also for multiple Bragg angle incidence. Alferness[14] and Poon and Korpel[15] have analyzed the diffraction efficiencies of thick holograms and AO interaction operating in the second-order Bragg regime. Exact solutions for the diffracted intensities of the zeroth, first, and second orders for this case (see Fig. 4 for geometry) exist in the literature for plane-wave incidence at twice the Bragg angle.[15] In what follows we compute the interaction transfer functions for these orders when an arbitrary optical field propagating nominally at twice the Bragg angle is incident on the AO modulator. In this case and limiting ourselves to three orders—*viz*., 0, 1, and 2—we can use Eqs. (9) and (10) to derive the following set of coupled equations between the spectra of the diffracted orders:

$$\frac{\partial\hat{\psi}_0}{\partial z} = \frac{j(k_x^2 - 4k\phi_B k_x)}{2k}\hat{\psi}_0 - \frac{j\alpha}{2L}\exp(-jk\delta z)\hat{\psi}_1, \quad (20)$$

$$\frac{\partial\hat{\psi}_1}{\partial z} = \frac{jk_x^2}{2k}\hat{\psi}_1 - \frac{j\alpha}{2L}\exp(jk\delta z)(\hat{\psi}_0 + \hat{\psi}_2), \quad (21)$$

$$\frac{\partial\hat{\psi}_2}{\partial z} = \frac{j(k_x^2 + 4\phi_B k k_x)}{2k}\hat{\psi}_{-1} - \frac{j\alpha}{2L}\exp(-jk\delta z)\hat{\psi}_1, \quad (22)$$

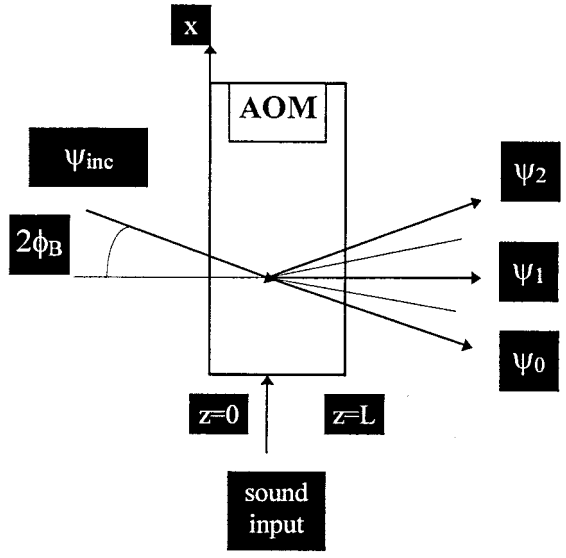

Fig. 4. Configuration showing light incidence at twice the Bragg angle during AO interaction, along with the diffracted orders.

where all the parameters have been defined in Subsection 3.A. Using an iterative procedure similar to that presented in Subsection 3.A, we compute the transfer functions of the zeroth, first, and second orders. The incident-beam profiles were again taken to be a rect$(\cdots)$ function and a Gaussian function, and identical transfer functions were computed from both input conditions, as expected. The magnitude plots of the transfer functions are plotted in Fig. 5 for $Q = 14$. It is interesting to note that single-sided notch filtering occurs if the zeroth order is used for image filtering. Note that the location of the notch for $k_x > 0$ in the transfer function of the undiffracted order again appears around the same location as in Fig. 2, i.e., at the Bragg angle. Physically, the plane waves around the Bragg angle have been diffracted into the first order as indicated in Fig. 5. To confirm our results, we have checked the dependence of the peak of the transfer function (indicative of the power in the second diffracted order) for the second order on the peak phase delay α and for $Q = 14$. The results

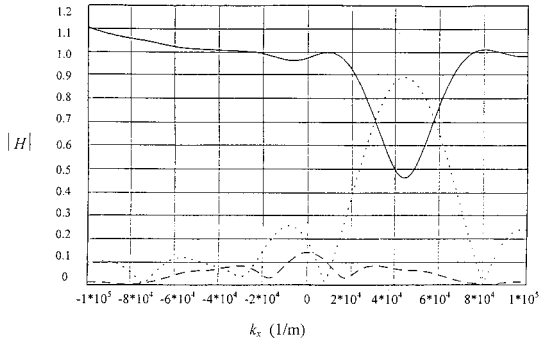

Fig. 5. Computed transfer functions for zeroth (solid curve), first (dotted curve), and second (dashed curve) orders for incidence at twice the Bragg angle. The parameters are $\alpha = 0.7\pi$, $Q = 14$, and $\lambda_0 = 632.8$ nm.

are in close agreement with the dependence of the plane-wave diffraction efficiency on α for second-order incidence, as calculated by Poon and Korpel,[15] which, in turn, is close to experimental results.

4. Conclusion

We have presented numerical procedures for the calculation of the spatial transfer functions for AO image processing. When the optical image is incident normally on the AO modulator, double-sided notch spatial filtering occurs. For an optical image incident at twice the Bragg angle, single-sided notch filtering results. Finally, note that, although we discuss spatial filtering along one transverse dimension in this paper, the procedure can readily be extended to two transverse dimensions by use of adjacent AO cells with orthogonally propagating sound along x and y, as discussed in Ref. 8.

References

1. H. K. Liu, J. Davis, and R. Lilly, "Optical-data-processing properties of a liquid-crystal television spatial light modulator," Opt. Lett. **10,** 635–637 (1985).
2. J. Grinberg, A. Jacobson, W. Bleha, L. Miller, L. Fraas, D. Boswell, and G. Myer, "A new real-time non-coherent to coherent light image converter: the hybrid field effect liquid crystal light valve," Opt. Eng. **14,** 217–225 (1975).
3. W. E. Ross, D. Psaltis, and R. Anderson, "Two-dimensional magneto-optic spatial light modulator for signal processing," Opt. Eng. **22,** 485–490 (1983).
4. A. VanderLugt, *Optical Signal Processing* (Wiley, New York, 1992).
5. P. Das and C. DeCusatis, *Acousto-Optic Signal Processing: Fundamentals & Applications* (Artech House, New York, 1991).
6. A. Korpel, *Acousto-Optics*, 2nd ed. (Artech House, New York, 1997).
7. J. Xia, D. B. Dunn, T.-C. Poon, and P. P. Banerjee, "Image edge enhancement by Bragg diffraction," Opt. Commun. **128,** 1–7 (1996).
8. P. P. Banerjee, D. Cao, and T.-C. Poon, "Basic image-processing operations by use of acousto-optics," Appl. Opt. **36,** 3086–3089 (1997).
9. D. Cao, P. P. Banerjee, and T.-C. Poon, "Image edge enhancement with two cascaded acousto-optic cells with contrapropagating sound," Appl. Opt. **37,** 3007–3014 (1998).
10. M. R. Chatterjee, T.-C. Poon, and D. N. Sitter, Jr., "Transfer function formalism for strong acousto-optic Bragg diffraction of light beams with arbitrary profiles," Acustica **71,** 81–92 (1990).
11. M. D. McNeill and T.-C. Poon, "Gaussian-beam profile shaping by acousto-optic Bragg diffraction," Appl. Opt. **33,** 4508–4515 (1994).
12. R. J. Pieper and T.-C. Poon, "System characterization of apodized acousto-optic Bragg cells," J. Opt. Soc. Am. A **7,** 1751–1758 (1990).
13. P. P. Banerjee and C. W. Tarn, "A Fourier transform approach to acousto-optic interactions in the presence of propagational diffraction," Acustica **74,** 181–191 (1991).
14. R. Alferness, "Analysis of propagation at the second-order Bragg angle of a thick holographic grating," J. Opt. Soc. Am. **66,** 353–362 (1976).
15. T.-C. Poon and A. Korpel, "High efficiency acousto-optic diffraction into the second Bragg order," in *IEEE Ultrasonics Symposium Proceedings* (Institute of Electrical and Electronics Engineers, New York, 1983), pp. 751–754.